Fuel 254 (2019) 115714

Contents lists available at ScienceDirect

Fuel

journal homepage: www.elsevier.com/locate/fuel

Full Length Article

Steam reforming of acetic acid over Ni-based catalysts derived from $La_{1-x}Ca_xNiO_3$ perovskite type oxides

Roberto B.S. Junior[a], R.C. Rabelo-Neto[b], Ruan S. Gomes[c], F.B. Noronha[b], Roger Fréty[c], Soraia Teixeira Brandão[c,*]

[a] LCCP – Laboratory of Catalysis and Catalytic Processes, Dipartimento di Energia, Politecnico di Milano, Piazza Leonardo da Vinci 32, 20133 Milano, Italy
[b] Instituto Nacional de Tecnologia, Av. Venezuela 82, 20081-312 Rio de Janeiro, Brazil
[c] Universidade Federal da Bahia, Instituto de Química, Rua Barão de Jeremoabo, 147, Ondina, CEP: 40170-115 Salvador, BA, Brazil

ARTICLE INFO

Keywords:
Ni-based
Calcium substitution
Steam reforming
Syngas generation

ABSTRACT

Ni/CaO-La_2O_3 catalysts generated by in situ reduction of $La_{1-x}Ca_xNiO_3$ perovskite systems (x = 0; 0.15; 0.30 and 0.50) were prepared and evaluated in steam reforming of acetic acid under steady state conditions. The objective of this work was to study the effect of calcium content towards activity and syngas formation in such catalytic systems. The catalytic materials were characterized by in situ X-ray diffraction and temperature programmed reduction. The catalytic activity was evaluated in a packed bed reactor in a temperature range from 400 to 700 °C for $LaNiO_3$ reduced samples and at 600 °C for the $La_{1-x}Ca_xNiO_3$ reduced precursors. The tests indicated that the presence of calcium oxide directly promotes hydrogen formation, by permitting a greater amount of water to be converted and limits the occurrence of ketonization.

1. Introduction

The abrupt climate changes caused by global warming and the non-stoppable ever-increasing energy consumption are complex challenges humankind must urgently deal with. The extreme dependence of up-to-date energy production technologies on non-renewable sources had been of negative effect on environmental and energy security issues [1]. Environmentally, in order to maintain the present standard of living, producing energy from non-renewable sources is unsustainable as it is directly or indirectly correlated to large amounts of greenhouse gases [1,2]. Economically, the establishment of a competitive energetic matrix, minimally dependent on foreign oil-based sources, is a matter of national sovereignty and of external political relationships [3,4]. A viable solution for the problem presented above could be the development of the so-called hydrogen economy, in which hydrogen would be inserted in the energetic matrices, diminishing crude-oil participation.

Hydrogen is considered an important energetic vector for the future generations and its production techniques have been exhaustively studied in the literature [5–9]. This important energy source can be produced by various routes as exemplified by coal and biomass gasification [6,7,10], steam reforming and partial oxidation of ethanol and the consolidated catalytic steam reforming of methane [11–15]. An interesting process that has called attention recently is the steam reforming of bio-oil produced by different types of biomass transformation. Bio-oil is a complex mixture of at least 200 different compounds, including acids, aldehydes, ketones, alcohols and lignin oligomers emulsified in aqueous medium [16–20]. Biomass derived liquids composition is fully dependent of the biomass origin and the applied technology used on its conversion. Due to the complexity of bio-oil composition and to the fact that the catalytic phenomena are utterly correlated to the substrate/surface interactions, authors have studied the catalytic activation of its major component, acetic acid, which can have a 12–14 wt% content in bio-oil [18,21,22].

The steam reforming of acetic acid is presented by Eq. (1):

$$CH_3COOH + 2H_2O \rightarrow 2CO_2 + 4H_2 \quad (1)$$

Steam reforming of acetic acid has been studied on different catalytic systems, such as supported noble metals [5,23,24]. Supported noble metals catalysts showed themselves quite active and relatively stable against coke formation, but these systems have the disadvantage to be quite expensive when compared to nickel and copper-based materials [16,25]. The advantage in using nickel-containing catalysts is due to its low price and relatively high availability if compared with noble metals. It has been reported that nickel-based catalysts are as active as noble metal systems but deactivation phenomena due to coke formation is still a problem to be deeper understood in those systems. To better understand the effect of the synthesis route on the steam

* Corresponding author.
E-mail address: brandao@ufba.br (S.T. Brandão).

https://doi.org/10.1016/j.fuel.2019.115714
Received 28 March 2019; Received in revised form 19 June 2019; Accepted 24 June 2019

reforming of acetic acid, Xiang and co-workers [26] have synthesized diverse batches of Ni/γ-Al_2O_3 using nitrate, chlorate, acetate and Sulphur-containing nickel precursors calcined at 600 °C. The work demonstrated the inadequacy of S-containing synthesis routes due to nickel silicate formation and the interaction of alumina with chlorine revealed to be the main reason to the support's sintering. The acetate and nitrate routes produced Ni-based catalysts with similar activity towards syngas production, being the coke formation still an issue. Lee and co-workers [27] have evaluated the effect of Ni/γ-Al_2O_3 catalyst promotion with Mg, La, K and Cu dopants on acetic acid conversion and coke suppression. Mg doping was shown to suppress coke formation circa 60% by comparison with unpromoted Ni/γ-Al_2O_3 and the presence of lanthanum and potassium seemed to have contributed to an increase in the total catalyst's basicity. Still on the evaluation of the effect of synthesis route on the final performance of Ni-based catalysts, Lago and co-workers [28] have verified that destruction of ABO_3 perovskite-type precursors in a reducing atmosphere, prior to the reaction, could generate a B^0/A_2O_3 catalyst with B^0 metallic particles finely dispersed on A_2O_3 oxide. During the last decade Noronha and co-workers have been studying the application of perovskite-type oxides on syngas production [29–33]. Specifically, on steam reforming of acetic acid, a positive effect of La-site substitution by Pr and Sm was observed on the suppression of coke formation, without significative effect on acetic acid conversion. The authors agreed that the tradeoff between rare earth's elevated cost and their activity respect to acetic acid conversion makes their large-scale utilization not feasible.

In the present work, nickel-based catalysts were obtained in situ, by hydrogen reducing treatment of the $La_{1-x}Ca_xNiO_3$ system and their activity towards syngas and stability due to coking formation were evaluated in the steam reforming of acetic acid during 23 h time on stream (TOS).

2. Experimental

2.1. Synthesis of the catalyst's precursors.

Perovskites $La_{1-x}Ca_xNiO_3$ (x = 0, 0.15, 0.30, 0.50) were prepared by citrate method [34]. This method consists in a simple dissolution of stoichiometric amounts of metallic nitrates, together with an excess of citric acid, that is introduced to guarantee first the formation of the gel-like viscous syrup after water evaporation and finally, the formation of the glassy material that will be calcined in further steps [35]. Stoichiometric quantities of lanthanum, calcium and nickel nitrates were dissolved in water, then citric acid was added to this solution, being the ratio between citric acid molar amount and total molar amount of metallic ions equal to 1.5. The solution was heated for 1 h at 90 °C until the formation of a gel that immediately was calcined in air in different steps: 100 °C for 1 h; 300 °C for 2 h; 800 °C for 4 h, always with heating rate equal to 10 °C/min. The non-Ca containing perovskite was named $LaNiO_3$ and the calcium-containing samples were named Ca 15%, Ca 30% and Ca 50% (molar fraction based).

2.2. Characterization

X-Ray Powder Diffraction (XRD) analyses of the calcined samples were conducted at room temperature with Cu Kα radiation (λ = 1.5418 Å) using a Shimadzu XRD-6000 diffractometer. Data were collected in the 2θ range of 10° to 80°, with a scan rate of 0.25°/min. Temperature programmed reduction (TPR) analysis was performed by reducing an amount of 20 mg of perovskite diluted with 20 mg of quartz powder in a flow of 30 mL/min (5% H_2/He) from room temperature until 800 °C at a ramping rate of 10 °C/min and the hydrogen consumption was monitored by mass spectrometry (Balzer, model QMS 200). In situ diffraction experiments were conducted in a furnace installed into a Huber goniometer operating in Bragg–Brentano geometry at the D10B-XPD beamline at the Laboratório Nacional de Luz Síncrotron at Campinas – São Paulo, using a radiation with λ = 1.5500 Å. The analyses were performed during the reduction of the catalyst precursors under a flow of 30 mL/min of 5% H_2/He mixture.

2.3. Steam reforming of acetic acid

Steam reforming (SR) of acetic acid was performed in a fixed-bed reactor using a Microactivity Reference equipment (PID Eng & Tech.) previously described in [29,30]. The samples (10 mg of catalyst diluted in 150 mg of SiC) were previously reduced with 30 mL/min pure H_2 stream at 800 °C for 1 h. The reactant mixture containing a water/acetic acid ratio of 3 on molar basis was pumped (0.25 mL/min) into a vaporizer and diluted with He (200 mL/min) and then, it was fed to the reactor. Initial proof experiments and thermodynamic calculations presented in topic 3.3 were performed to determine the range of temperature for the catalytic tests in order to minimize carbon formation. Being so, $LaNiO_3$ catalyst were evaluated from 400 to 700 °C and the Ca-containing catalysts at 600 °C. Reactants and products were analyzed by gas chromatography (Agilent 7890A) equipped with a thermal conductivity detector (TCD) and a Porapak Q column.

Eqs. (2), 3 and 4 were used to calculate conversion, compositions, molar flow in the entrance (n^{inlet}) and outlet (n^{outlet}) of the reactor.

$$\textit{Conversion of reactant } i\text{: } X_i = 100 * \frac{n_i^{inlet} - n_i^{outlet}}{n_i^{inlet}} \quad (2)$$

$$\textit{Composition of product } i\text{: } Y_i = 100 * \frac{n_i^{outlet}}{n_{total}^{outlet}} \quad (3)$$

$$n_{total}^{outlet} = \sum n_i^{outlet},\ i = \textit{Acetic acid, } H_2O, H_2, CO, CO_2, CH_4 \textit{ and acetone} \quad (4)$$

3. Results and discussion

3.1. XRD, TPR and in situ X-ray diffraction studies.

Fig. 1 shows the XRD diffraction lines of the calcined $La_{1-x}Ca_xNiO_3$ samples.

XRD patterns of the calcined $LaNiO_3$ sample revealed the characteristic lines of $LaNiO_3$ rhombohedral phase (PDF 33-0711), as mentioned in literature [36], indicating that the perovskite structure is the main phase obtained after calcination for the Ca-free sample (x = 0). The substitution of Lanthanum by Calcium resulted in the appearance of segregated La_2NiO_4 (PDF 34-0314), CaO (PDF 03-1123)

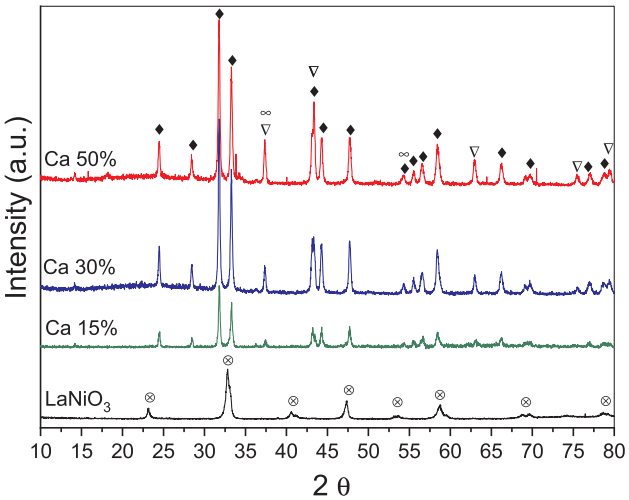

Fig. 1. XRD profiles of $La_{1-x}Ca_xNiO_3$ calcined system. ⊗: $LaNiO_3$; ◆: La_2NiO_4; ∇: NiO; ∞: CaO (λ = 1.5418 Å).

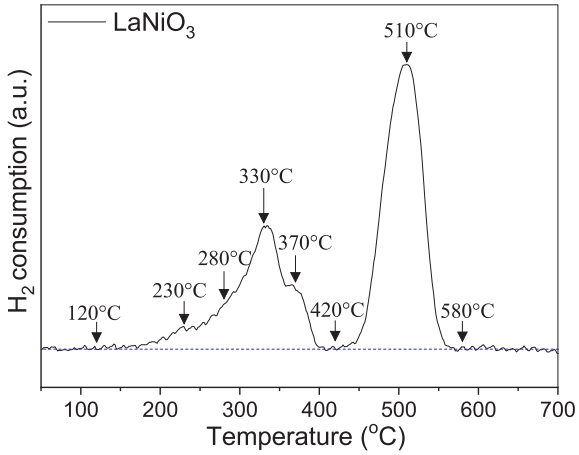

Fig. 2. TPR-H_2 profile of $LaNiO_3$ calcined precursor and the chosen temperatures for further in situ XRD experiments.

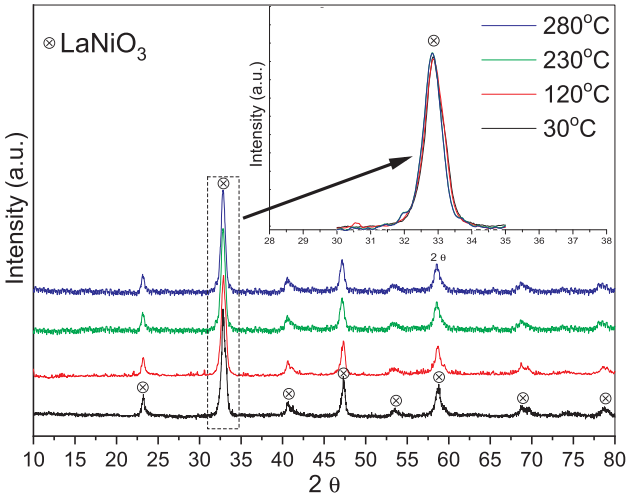

Fig. 3. In situ XRD profiles of $LaNiO_3$ on reducing atmosphere. 30 to 280 °C.

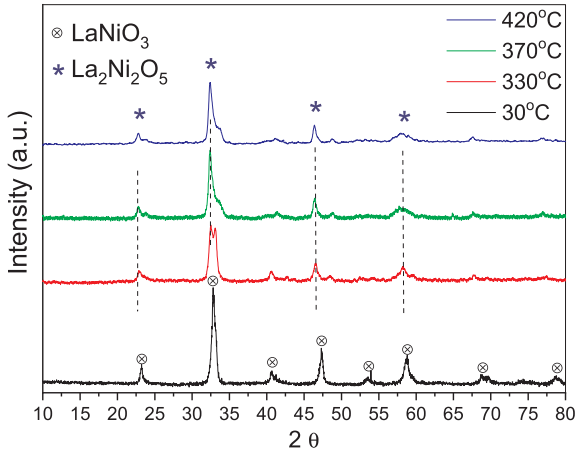

Fig. 4. In situ XRD profiles of $LaNiO_3$ on reducing atmosphere. 330 to 420 °C.

and NiO (PDF 44-1159). Lima and co-workers [34] have showed that values of $x \geq 0.1$ on $La_{1-x}Ca_xNiO_3$ system unfavored the formation of the perovskite-type structures, giving path to the segregation of part of the cations into NiO, CaO and La_2NiO_4 spinel. Fig. 2 shows the $LaNiO_3$ TPR-H_2 profile and some of the temperatures retained for in situ XRD studies ($\lambda = 1.5418$ Å) presented by the Figs. 3–5.

The reduction profile for $LaNiO_3$ (Fig. 2) shows four events. The first

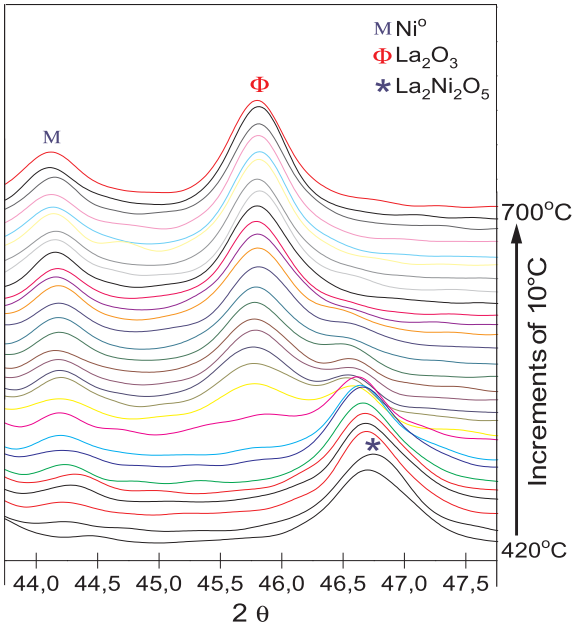

Fig. 5. In situ XRD profiles of $LaNiO_3$ on reducing atmosphere. 420 to 700 °C.

event starts at 171 °C followed by a shoulder at 230 °C that is rapidly superimposed to a peak with its maximum value at 330 °C. Until 280 °C as shown in Fig. 3, there is no detectable difference between the corresponding diffractograms, indicating that the initial hydrogen consumption could be correlated to the gradual oxygen loss until the maximum structural limit, with the formation of $LaNiO_{2,7}$, as proposed by Jia et al. [37]. The transformation presented by the perovskite between 280 °C and 420 °C can be verified in those diffractograms presented in Fig. 4 and corresponds to the reduction of Ni^{3+} to Ni^{2+}, forming $La_2Ni_2O_5$ (PDF 36-1230). This latter transformation is totally in agreement with the literature [38,39]. The difference between $LaNiO_3$ and $La_2Ni_2O_5$ (2θ = 26; 28,8; 29,86; 39,16) XRD profiles are very subtle as already shown by Valderrama et al [38]. The conversion from Ni^{2+} to Ni^0 is favoured at temperatures higher than 420 °C, as shown in Fig. 5, generating Ni^0 (PDF 00-001-1258) supported on lanthanum oxide (PDF 01-073-2141). TPR allied to in situ XRD measurements showed that the destruction of $La_2Ni_2O_5$ to generate Ni^0/La_2O_3 occurs in the 420–600 °C temperature range. The TPR profiles of $La_{1-x}Ca_xNiO_3$ precursors were significantly changed and shifted to higher temperatures as can be seen in Fig. 6.

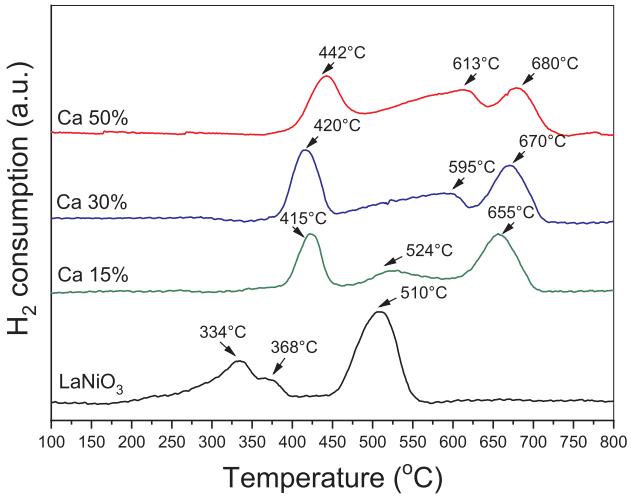

Fig. 6. TPR-H_2 profiles of $La_{1-x}Ca_xNiO_3$ calcined system.

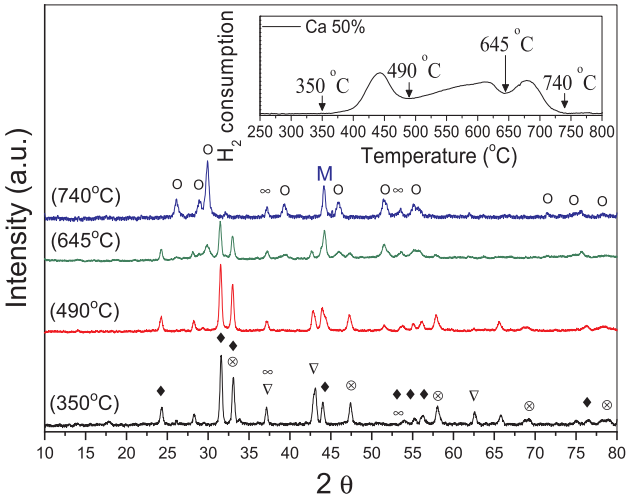

Fig. 7. In situ XRD profiles of Ca 50% at selected temperatures. ⊗ – $LaNiO_3$; ♦ – La_2NiO_4; ∇ – NiO; ∞ – CaO; M – Ni^0; O – La_2O_3.

These profiles presented a first peak of H_2 consumption at (400–440 °C), followed by a broad peak (450–620 °C) and a third peak at high temperature (650–670 °C). Attempting to obtain a better understanding also on the redox properties of those calcium-containing precursors, studies of in situ XRD were performed with Ca 50%. The results can be seen in Fig. 7. As a matter of fact, the analysis of Ca 50% can be extended to the other calcium-containing materials as the TPR profiles are quite similar.

For the $La_{0.5}Ca_{0.5}NiO_3$ precursor, the diffractogram obtained after reduction at 490 °C showed that the intensity of the diffraction lines characteristic of La_2NiO_4 phase decreased whereas weak lines due to La_2O_3 and metallic Ni were observed. In the TPR profile of this catalyst, the first hydrogen consumption (maximum at 440 °C) can be attributed to the reduction of segregated NiO, in agreement with the disappearance above 490 °C of the corresponding diffraction line (2Θ = 63°). In the presence of calcium (50%) La_2NiO_4 appears more stable at high temperature if compared to the Ca-free system. The TPR reduction peak above 645 °C is therefore attributed to the complete reduction of La_2NiO_4 [40,41]. Fig. 7 exhibits only the lines of La_2O_3 and metallic Ni after further increase of the reduction temperature up to 740 °C. Although the average size of La_2NiO_4 crystallites is apparently not affected by the Ca content, the average crystallite size of reduced nickel crystallites obtained after reduction of the catalysts is affected by the presence of Ca. the size of Ni° crystallites increases strongly when adding 15% of Ca in the $LaNiO_3$ perovskite, and then in a more moderate way when going from 15 to 50% of Ca. This increase in Ni° crystallite size when increasing Ca content is probably linked to the difficulty to fully reduce the catalysts as evidenced by TPR curves in Fig. 2. The maximum temperature of the final reduction process is 510, 655, 670, 680 °C for the catalysts containing respectively 0, 15; 30 and 50% Ca. The higher the final reduction temperature, the more difficult reduction, but the higher the Ni° diffusion rate, generating therefore larger Ni° crystallite sizes. The sintering of Ni crystallites is apparently not directly correlated to the crystallite size of the parent oxide structure, suggesting that the reduction destroy at least in part the spatial organization of the precursors. Then, together with an agglomeration of Ni° species during reduction, LaO_x species also reorganize to generate La_2O_3 based compounds associated in an unknown way to Ca species. As no change in metallic nickel phase diagram is observed after reduction, the amount of Ca inside Ni° structure must be negligible. Table 1 shows the average crystallite size of La_2NiO_4 found on calcium-containing calcined samples and the metallic Ni formed after reduction in situ at 800 °C, calculated by Debye Scherrer Equation, using the respective most intense diffraction lines (La_2NiO_4 at 2θ = 32 and Ni^0 at 2θ = 44,2).

Table 1
Average crystallite size of La_2NiO_4 and Ni^0 (reduction at 800 °C).

Precursor	La_2NiO_4 (nm)	Ni^0 (nm)
$LaNiO_3$	–	22
Ca 15%	38	40
Ca 30%	38	43
Ca 50%	35	47

The average size of La_2NiO_4 crystallites did not change significantly with calcium content, but the size of metallic nickel crystallites formed after "in situ" reduction, is clearly increased as the amount of Ca is increased.

3.2. Thermodynamic considerations and homogeneous reaction results.

In order to check the feasibility of hydrogen production from acetic acid steam reforming on the conditions previously detailed in the experimental section, thermodynamic data were calculated by Gibb's free energy minimization using a home-made code with Mathematica® software. It was considered the presence of carbon graphite in the equilibrium and the ideality for all the gaseous species. In the experimental conditions, the steam reforming of acetic acid leads only to hydrogen, acetone, methane, carbon dioxide and monoxide gaseous products and being so, the thermodynamic allowed conversion of acetic acid and water and the products composition (dry basis) are confronted with the homogeneous experimental results. The confrontation is shown in Fig. 8(A)–(C).

The complete conversion of acetic acid in this range of temperature is not limited by thermodynamics but its steam reforming in gas phase is kinetically unfavoured. The maximum conversion is reached only at 700 °C and it is below 10%. The conversion of water is even lower as can be seen in Fig. 8(A). In the equilibrium, as can be seen in Fig. 8(B), only traces of acetone and solid carbon were expected in the 400–700 °C range and the formation of hydrogen and carbon monoxide are favoured as the temperature increases. In the entire range of temperature acetic acid is not found in the equilibrium and at 400 °C it is fully decomposed in methane and carbon dioxide. The presence of hydrogen at low temperatures accompanies water and methane consumption, being the presence of the later directly correlated to the velocity in which the hydrogen is released. Once methane lacks in the system hydrogen tends to find its maximum yield and the concentration of water does not change anymore. The quantity of carbon expected by thermodynamics is irrelevant.

Homogeneous run is presented in Fig. 8(C). Carbon balances shows that the conversion of acetic acid is small but leads to a great formation of coke. The carbon containing substances in gas phase does not justify the quantity of acetic acid converted and only at 700 °C traces of gaseous products were detected.

3.3. $LaNiO_3$ evaluation–the effect of reaction temperature.

In order to understand the effect of temperature on catalytic steam reforming of acetic acid, $LaNiO_3$ sample was tested on 23 h TOS in a 400–700 °C range, with increments of 100 °C. The results of conversion and compositions are shown in Fig. 9.

The increment in temperature had a significant effect in acetic acid conversion and on products distribution. At 400 °C, the low acetic acid conversion leads almost completely to its ketonization product (Eq.8) and coke, and it is completely in agreement with the presence of carbon dioxide and acetone in gas phase.

Ketonization: $2CH_3COOH \rightarrow (CH_3)_2CO + H_2O + CO_2$ (8)

In the first hours of reaction the conversion of acetic acid is low but rapidly increases as hydrogen is being released in the system and this

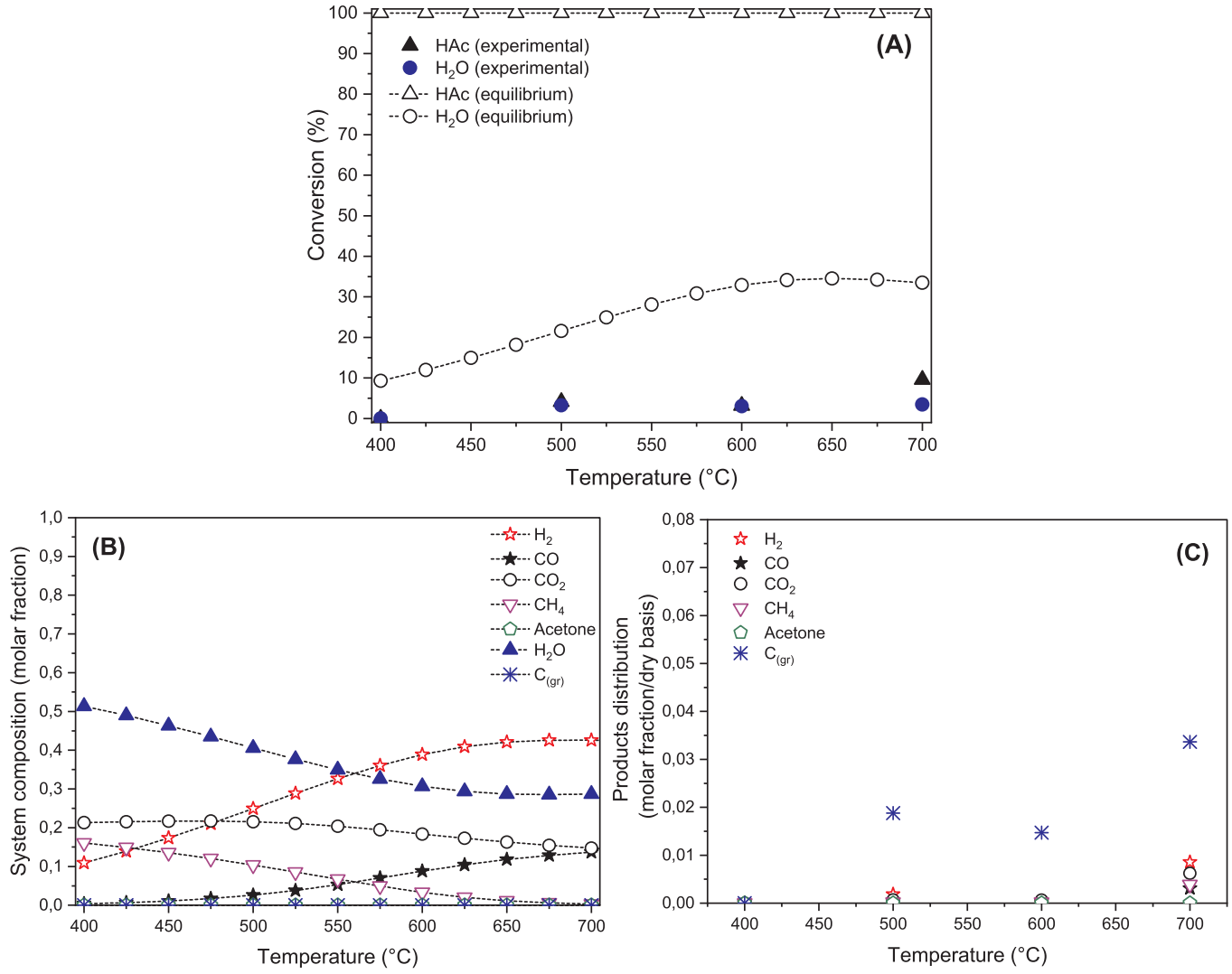

Fig. 8. (A) HAc and H_2O conversion (homogeneous run versus equilibrium), (B) System composition in the equilibrium and (C): Products distribution in the homogeneous run.

fact could be correlated to the oxido-reducing character of the gas composition. The gas composition at the beginning could partially re-oxidize the Ni^0 species and as hydrogen is been produced, nickel oxidized species tend to return to their original metallic state. At this temperature water conversion was very low and so are the yields of hydrogen and carbon monoxide.

When the temperature increases, the acetic acid conversion increases up to 600 °C. It should be pointed out that up to 600 °C the conversion of acetic acid has its steady state delayed as the temperature increases and it is achieved exactly when acetone concentration remains constant, also reaching its steady state condition. In all temperatures, excepted 400 °C, the conversion of acetic acid is at its maximum value at the beginning of the run, but rapidly decreases, due to catalyst deactivation. The deactivation observed, as Takanabe et al. reported [24], could be explained by coke formation that is directly correlated to the presence of acetone in the system. Acetone could suffer aldol-condensation type reactions forming coke deposits [24]. The molar fraction of carbon was calculated by mass balance and is presented in Fig. 10.

As already presented in Fig. 9, acetic acid conversion has no thermodynamic limitations and due to kinetic effects, it could also generate carbon deposits on the catalyst. The Fig. 11 shows the potentiality of acetic acid ketonization occurrence in the experimental conditions stablished in this work.

$$K = \frac{p_{acetone} * p_{H2O} * p_{CO2}}{p^2_{acetic\ acid}} \quad (9)$$

The constant K_{exp} (experimental) and K_{eq} (equilibrium) are calculated using (Eq. (9)). The former was calculated using the experimental partial pressures verified during the tests and the later using thermodynamic data. In all experiments the K_{exp}/K_{eq} ratio is lower than 1, meaning that the formation of acetone is favoured by thermodynamics during the entire run, no matter the temperature.

The presence of methane at 700 °C is higher than in any other reaction temperature during the first hours of run and its presence is attributed to acetic acid decomposition [24]. Takanabe et al. proposed a kinetic scheme in which acetic acid decomposes into methane, CO_x and hydrogen, showing that the contribution in methane formation due to carbon monoxide hydrogenation is irrelevant. A bifunctional mechanism could be retained for the catalytic process, in which water could be activated by the support, generating hydroxyl groups that could be used in steam reforming or WGS reactions (Eq. (10)).

$$WGS:\ CO + H_2O \rightarrow CO_2 + H_2 \quad (10)$$

The acetic acid could be decomposed into hydrogen, methane, carbon monoxide and dioxide and CH_x species that could oligomerize, blocking catalytic sites and also could recombine to give path to acetone synthesis that is also raw material for oligomerization products.

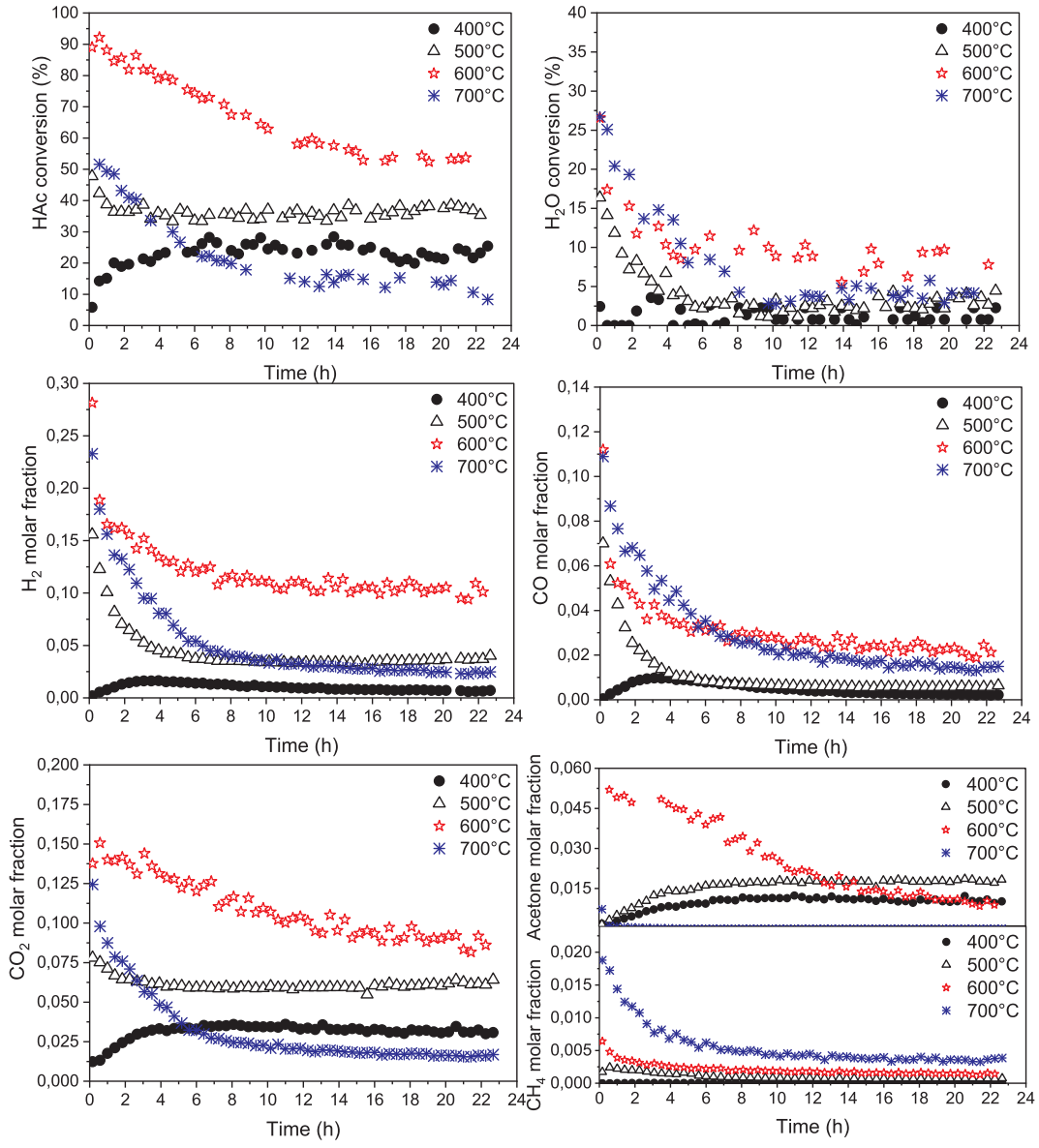

Fig. 9. Reduced $LaNiO_3$ evaluated on steam reforming of acetic acid at 400, 500, 600 and 700 °C.

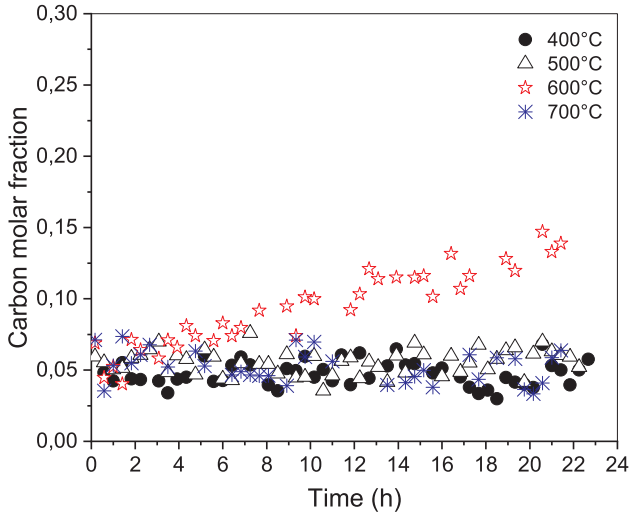

Fig. 10. Carbon molar fraction calculated by mass balance at 400, 500, 600 and 700 °C.

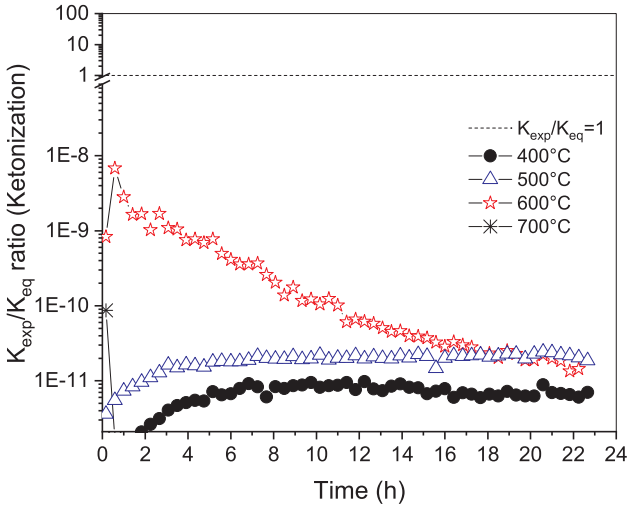

Fig. 11. Steam reforming of acetic acid: potential of ketone formation at different temperatures.

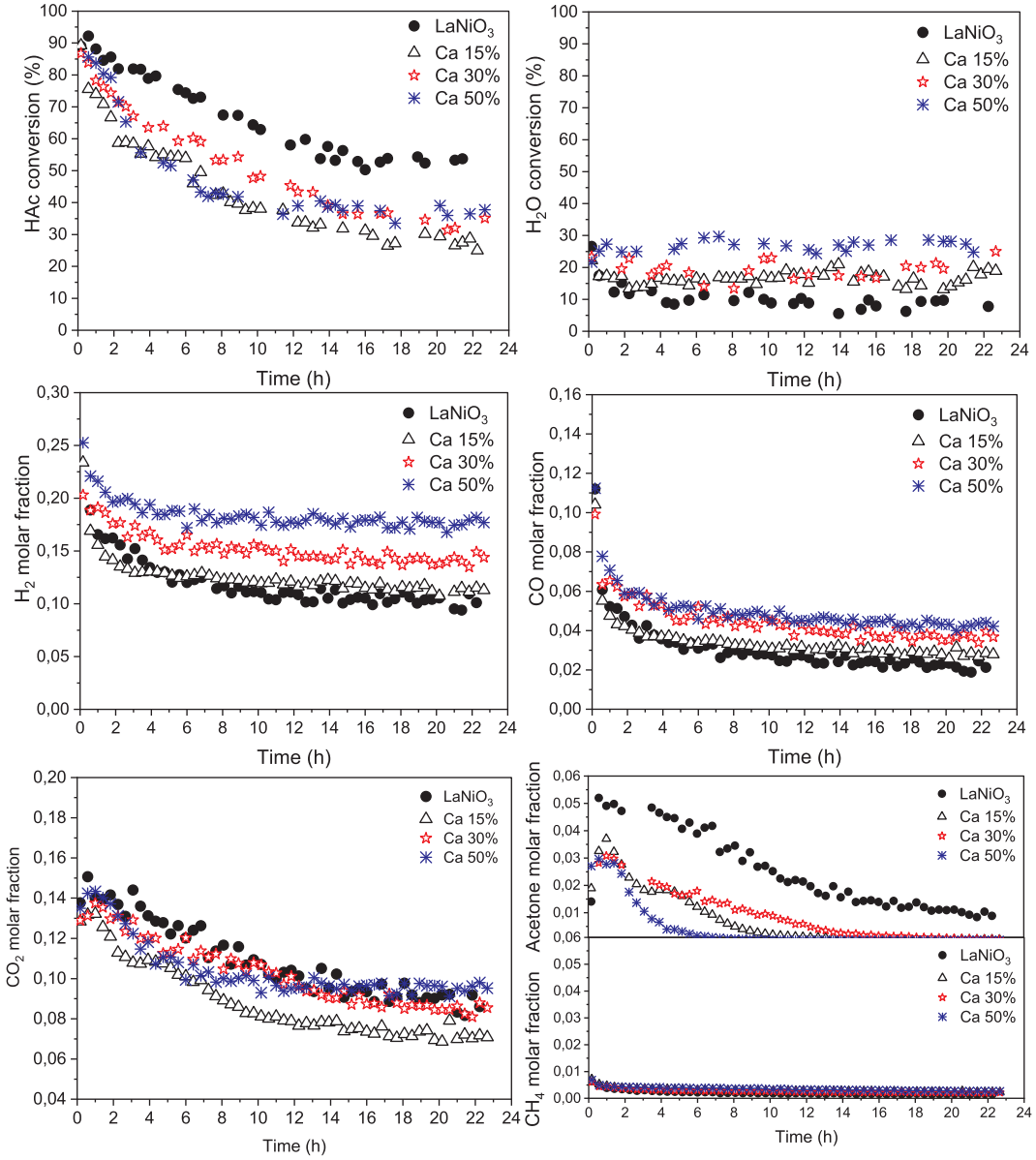

Fig. 12. $La_{1-x}Ca_xNiO_3$ reduced samples evaluated on steam reforming at 600 °C.

The activation of water on the support surface plays an important role not only in hydrogen formation step (recombination of hydrogen adsorbed atoms) but also in cleaning the active phase by hydrogenating those CH_x groups. The effect of support composition is studied in the next section.

3.4. Effect of calcium content in $La_{1-x}Ca_xNiO_3$.

The effect of calcium content on $La_{1-x}Ca_xNiO_3$ perovskites in the steam reforming of acetic acid and the activity of the corresponding catalysts is presented in Fig. 12.

The conversion of acetic acid presented by the calcium-containing catalysts is lower than the one achieved by the reduced $LaNiO_3$. Table 2 shows the values of the reactant's conversion achieved after 23 h TOS and the Ni^0 average crystalize size calculated by Debye Scherrer's Equation for all samples.

As can be seen in Table 2, a rather good correlation is observed between the conversion of acetic acid and the Ni^0 average crystallite size. The average diameter of Ni^0 crystallites when $LaNiO_3$ is reduced in situ is less than 50% of those obtained by reduction of calcium-containing catalysts and so, the metallic area accessible when calcium is present is approximately half of that accessible in the reduced $LaNiO_3$. The smaller is the active phase crystallite size, the higher is the presence of steps and kinks on its surfaces, increasing so the turnover rate [42] what could explain the higher acetic acid conversion on Ni/La_2O_3 obtained from $LaNiO_3$ precursor. The presence of calcium has a positive effect on water conversion, as can be seen in Table 2. It increases with calcium content and when calcium substitutes lanthanum in Ca 50%

Table 2
Steam reforming of acetic acid at 600 °C in presence of Ni-based catalysts issued from $La_xCa_{1-x}NiO_3$ precursors: conversion of both reactants after 23 h TOS and values of the mean crystallite size of reduced nickel. Ni^0 crystallite sizes from Table 1 are also recalled.

Precursor	Conversion of HAc (%)	Conversion of H_2O (%)	Ni^0 (nm)
$LaNiO_3$	52.8	7.0	22
Ca 15%	28.1	16.6	40
Ca 30%	33.2	20.5	43
Ca 50%	37.1	28.5	47

sample, the conversion of water increases by a factor of 4.

As it has already been mentioned, it is believed that steam reforming of acetic acid proceed via bifunctional mechanism, being the water activated on the support generating hydroxyl groups that could be recombined to give hydrogen and to slow down the deactivation by steam reforming of those possible CH_x intermediates derived from acetic acid decomposition. In fact, the increase in calcium content showed an increase in water conversion and also a significant increase in hydrogen production. It could be inferred that the increase in calcium content produces a more efficient support for water activation. The presence of calcium seemed to mitigate acetic acid conversion to acetone and the increase in calcium content makes acetone depletion come sooner with time on stream. The system containing reduced $LaNiO_3$ displayed detectable acetone during the entire 23 h TOS but in those systems containing calcium, acetone formation was pulled back and its presence could not be detected after 5 h TOS in presence of Ca50%.

4. Concluding remarks

The catalysts generated in situ were active when applied to the steam reforming of acetic acid. XRD studies showed that the presence of calcium increased significantly the Ni^0 crystallite average size. The presence of calcium seemed to anticipate both production and complete depletion of acetone, an undesired side product that is the precursor of carbon solid structures that could accelerate the catalyst deactivation. It was possible to verify a linear correlation between Ca content and the conversion of water, being the presence of the former beneficial to water activation. Hydrogen and carbon monoxide generation was also directly proportional to Ca content.

Acknowledgements

The authors acknowledge the Brazilian Synchrotron Light Laboratory for the acceptance of missions D10B-XPD 9253 and 10799.

References

[1] Xu X, Li P, Shen Y. Small-scale reforming of diesel and jet fuels to make hydrogen and syngas for fuel cells: a review. Appl. Energy 2013;108:202–17. https://doi.org/10.1016/j.apenergy.2013.03.028.

[2] Nazim Z, Muradov T, Veziroğlu Nejat. “Green” path from fossil-based to hydrogen economy: an overview of carbon-neutral technologies. Int. J. Hydrogen Energy 2008;33:6804–39. https://doi.org/10.1016/j.ijhydene.2008.08.054.

[3] Alessandra S, Wouter N, Rocco DM, Alessandro C, Maurizio G, Thiel C. How far away is hydrogen? Its role in the medium and long-term decarbonisation of the European energy system. Int. J. Hydrogen Energy 2015;41:19–35. https://doi.org/10.1016/J.IJHYDENE.2015.09.004.

[4] Wang Y, Holladay JD, Hu J, King DL. An overview of hydrogen production technologies. Catal. Today 2009;139:244–60.

[5] Basagiannis AC, Verykios XE. Influence of the carrier on steam reforming of acetic acid over Ru-based catalysts. Appl. Catal. B Environ. 2008;82:77–88. https://doi.org/10.1016/j.apcatb.2008.01.014.

[6] Cheng F, Dupont V. Nickel catalyst auto-reduction during steam reforming of bio-oil model compound acetic acid. Int. J. Hydrogen Energy 2013;38:15160–72. https://doi.org/10.1016/j.ijhydene.2013.09.111.

[7] Matasguell B, Babich I, Seshan K, Lefferts L. Steam reforming of biomass based oxygenates—mechanism of acetic acid activation on supported platinum catalysts. J. Catal. 2008;257:229–31. https://doi.org/10.1016/j.jcat.2008.04.019.

[8] Costa DS, Gomes RS, Rodella CB, da Silva RB, Fréty R, Teixeira Neto É, et al. Study of nickel, lanthanum and niobium-based catalysts applied in the partial oxidation of methane. Catal. Today 2018. https://doi.org/10.1016/j.cattod.2018.10.022.

[9] Rodrigues LMTS, Silva RB, Rocha MGC, Bargiela P, Noronha FB, Brandão ST. Partial oxidation of methane on Ni and Pd catalysts: influence of active phase and CeO_2 modification. Catal. Today 2012;197:137–43. https://doi.org/10.1016/j.cattod.2012.07.031.

[10] Howaniec N, Smoliński A. Effect of fuel blend composition on the efficiency of hydrogen-rich gas production in co-gasification of coal and biomass. Fuel 2014;128:442–50. https://doi.org/10.1016/j.fuel.2014.03.036.

[11] Duarte RB, Nachtegaal M, Bueno JMC, van Bokhoven JA. Understanding the effect of Sm_2O_3 and CeO_2 promoters on the structure and activity of Rh/Al_2O_3 catalysts in methane steam reforming. J. Catal. 2012;296:86–98. https://doi.org/10.1016/j.jcat.2012.09.007.

[12] Mondal KC, Ramesh Chandran S. Evaluation of the economic impact of hydrogen production by methane decomposition with steam reforming of methane process. Int. J. Hydrogen Energy 2014;39:9670–4. https://doi.org/10.1016/j.ijhydene.2014.04.087.

[13] Nieva MA, Villaverde MM, Monzón A, Garetto TF, Marchi AJ. Steam-methane reforming at low temperature on nickel-based catalysts. Chem. Eng. J. 2014;235:158–66. https://doi.org/10.1016/j.cej.2013.09.030.

[14] Barroso MN, Gomez MF, Arrúa LA, Abello MC. Co catalysts modified by rare earths (La, Ce or Pr) for hydrogen production from ethanol. Int. J. Hydrogen Energy 2014;39:8712–9. https://doi.org/10.1016/j.ijhydene.2013.12.043.

[15] Silva AM, de Farias AMD, Costa LOO, Barandas APMG, Mattos LV, Fraga MA, et al. Partial oxidation and water–gas shift reaction in an integrated system for hydrogen production from ethanol. Appl. Catal. A Gen. 2008;334:179–86. https://doi.org/10.1016/j.apcata.2007.10.004.

[16] Mohanty P, Patel M, Pant KK. Hydrogen production from steam reforming of acetic acid over Cu–Zn supported calcium aluminate. Bioresour. Technol. 2012;123:558–65. https://doi.org/10.1016/j.biortech.2012.07.019.

[17] Gao N, Li A, Quan C. A novel reforming method for hydrogen production from biomass steam gasification. Bioresour. Technol. 2009;100:4271–7. https://doi.org/10.1016/j.biortech.2009.03.045.

[18] Slinn M, Kendall K, Mallon C, Andrews J. Steam reforming of biodiesel by-product to make renewable hydrogen. Bioresour. Technol. 2008;99:5851–8. https://doi.org/10.1016/j.biortech.2007.10.003.

[19] Batista da Silva R, Brandão ST, Lucotti A, Tommasini MS, Castiglioni C, Groppi G, et al. Chemical pathways in the partial oxidation and steam reforming of acetic acid over a $Rh\text{-}Al_2O_3$ catalyst. Catal. Today 2017;289:162–72. https://doi.org/10.1016/j.cattod.2016.08.018.

[20] Pagani D, da Silva RB, Moioli E, Donazzi A, Lucotti A, Tommasini M, et al. Annular reactor testing and Raman surface characterization of the CPO of i-octane and n-octane on Rh based catalyst. Chem. Eng. J. 2016;294:9–21. https://doi.org/10.1016/j.cej.2016.02.090.

[21] Demirbaş A, Akdeniz F. Fuel analyses of selected oilseed shells and supercritical fluid extraction in alkali medium. Energy Convers. Manage. 2002;43:1977–84. https://doi.org/10.1016/S0196-8904(01)00144-3.

[22] Branca C, Giudicianni P, Di Blasi C. GC/MS characterization of liquids generated from low-temperature pyrolysis of wood. Ind. Eng. Chem. Res. 2003;42:3190–202. https://doi.org/10.1021/ie030066d.

[23] Basile A, Gallucci F, Iulianelli A, Borgognoni F, Tosti S. Acetic acid steam reforming in a Pd–Ag membrane reactor: the effect of the catalytic bed pattern. J. Membr. Sci. 2008;311:46–52. https://doi.org/10.1016/j.memsci.2007.11.033.

[24] Takanabe K, Aika K, Seshan K, Lefferts L. Catalyst deactivation during steam reforming of acetic acid over Pt/ZrO_2. Chem. Eng. J. 2006;120:133–7. https://doi.org/10.1016/j.cej.2006.04.001.

[25] Hu X, Lu G. Investigation of steam reforming of acetic acid to hydrogen over Ni–Co metal catalyst. J. Mol. Catal. A Chem. 2007;261:43–8. https://doi.org/10.1016/j.molcata.2006.07.066.

[26] Yu Z, Hu X, Jia P, Zhang Z, Dong D, Hu G, et al. Steam reforming of acetic acid over nickel-based catalysts: the intrinsic effects of nickel precursors on behaviors of nickel catalysts. Appl. Catal. B Environ. 2018;237:538–53. https://doi.org/10.1016/j.apcatb.2018.06.020.

[27] Choi I-H, Hwang K-R, Lee K-Y, Lee I-G. Catalytic steam reforming of biomass-derived acetic acid over modified $Ni/\gamma\text{-}Al_2O_3$ for sustainable hydrogen production. Int. J. Hydrogen Energy 2019;44:180–90. https://doi.org/10.1016/j.ijhydene.2018.04.192.

[28] Peña MA, Fierro JLG. Chemical structures and performance of perovskite oxides. Chem. Rev. 2001;101:1981–2018. https://doi.org/10.1021/cr980129f.

[29] Resende KA, Ávila-Neto CN, Rabelo-Neto RC, Noronha FB, Hori CE. Thermodynamic analysis and reaction routes of steam reforming of bio-oil aqueous fraction. Renew. Energy 2015;80:166–76. https://doi.org/10.1016/j.renene.2015.01.057.

[30] Resende KA, Ávila-Neto CN, Rabelo-Neto RC, Noronha FB, Hori CE. Hydrogen production by reforming of acetic acid using La–Ni type perovskites partially substituted with Sm and Pr. Catal. Today 2015;242:71–9. https://doi.org/10.1016/j.cattod.2014.07.013.

[31] da Silva AAA, da Costa LOO, Mattos LV, Noronha FB. The study of the performance of Ni-based catalysts obtained from $LaNiO_3$ perovskite-type oxides synthesized by the combustion method for the production of hydrogen by reforming of ethanol. Catal. Today 2013;213:25–32. https://doi.org/10.1016/j.cattod.2013.04.033.

[32] Rabelo-Neto RC, Sales HBE, Inocêncio CVM, Varga E, Oszko A, Erdohelyi A, et al. CO_2 reforming of methane over supported $LaNiO_3$ perovskite-type oxides. Appl. Catal. B Environ. 2018;221:349–61. https://doi.org/10.1016/j.apcatb.2017.09.022.

[33] Santos M de S, Neto RCR, Noronha FB, Bargiela P, da Rocha M da GC, Resini C, Carbó-Argibay E, Fréty R, Brandão ST. Perovskite as catalyst precursors in the partial oxidation of methane: The effect of cobalt, nickel and pretreatment. Catal. Today 2018;299:229–41. https://doi.org/10.1016/j.cattod.2017.06.027.

[34] de Lima SM, Peña MA, Fierro JLG, Assaf JM. Perovskites as catalyst precursors: partial oxidation of methane on $La_{1-x}Ca_xNiO_3$. Stud. Surf. Sci. Catal. 2007:481–6. https://doi.org/10.1016/S0167-2991(07)80178-9.

[35] Tascón JMD, Mendioroz S, Tejuca LG. Preparation, characterization and catalytic properties of $LaMeO_3$ oxides. Zeitschrift Für Phys. Chem. 1981;124:109–27. https://doi.org/10.1524/zpch.1981.124.1.109.

[36] Le NTH, Calderón-Moreno JM, Popa M, Crespo D, Van Hong L, Phuc NX. $LaNiO_3$ nanopowder prepared by an ‘amorphous citrate’ route. J. Eur. Ceram. Soc. 2006;26:403–7. https://doi.org/10.1016/j.jeurceramsoc.2005.06.004.

[37] Jia L, Li J, Fang W. Effect of H_2/CO_2 mixture gas treatment temperature on the activity of $LaNiO_3$ catalyst for hydrogen production from formaldehyde aqueous

solution under visible light. J. Alloys Compd. 2010;489:L13–6. https://doi.org/10.1016/j.jallcom.2009.09.104.
[38] Valderrama G, Goldwasser MR, Pietri E, Zurita MJP, Cubeiro ML, Navarro CU. Caracterización de perovskitas La1-xSrxNiO3 y La2-2xSr2xNiO4-d obtenidos a partir del método de auto-combustión, INCI. 30 (2005) 25–33.
[39] Pereñíguez R, González-DelaCruz VM, Holgado JP, Caballero A. Synthesis and characterization of a $LaNiO_3$ perovskite as precursor for methane reforming reactions catalysts. Appl. Catal. B Environ. 2010;93:346–53. https://doi.org/10.1016/j.apcatb.2009.09.040.
[40] Barros BS, Melo DMA, Libs S, Kiennemann A. CO_2 reforming of methane over La_2NiO_4/α-Al_2O_3 prepared by microwave assisted self-combustion method. Appl. Catal. A Gen. 2010;378:69–75. https://doi.org/10.1016/j.apcata.2010.02.001.
[41] Guo C, Zhang X, Zhang J, Wang Y. Preparation of La_2NiO_4 catalyst and catalytic performance for partial oxidation of methane. J. Mol. Catal. A Chem. 2007;269:254–9. https://doi.org/10.1016/j.molcata.2007.01.029.
[42] Christensen KO, Chen D, Lødeng R, Holmen A. Effect of supports and Ni crystal size on carbon formation and sintering during steam methane reforming. Appl. Catal. A Gen. 2006;314:9–22. https://doi.org/10.1016/j.apcata.2006.07.028.